THE JOURNAL OF PHYSICAL CHEMISTRY C

Article

pubs.acs.org/JPCC

O_2 Dissociation on M@Pt Core−Shell Particles for 3d, 4d, and 5d Transition Metals

Paul C. Jennings,[†,‡] Hristiyan A. Aleksandrov,[§,∥] Konstantin M. Neyman,*[,§,⊥] and Roy L. Johnston*[,#]

[†]School of Chemical Engineering and [#]School of Chemistry, University of Birmingham, Birmingham, United Kingdom

[§]Departament de Química Física and IQTCUB, Universitat de Barcelona, Barcelona, Spain

[∥]Faculty of Chemistry and Pharmacy, University of Sofia, Sofia, Bulgaria

[⊥]Institució Catalana de Recerca i Estudis Avançats (ICREA), Barcelona, Spain

Supporting Information

ABSTRACT: Density functional theory calculations are performed to investigate oxygen dissociation on 38-atom truncated octahedron platinum-based particles. This study progresses our previous work (Jennings et al. *Nanoscale*, 2014, **6**, 1153), where it was shown that flexibility of the outer Pt shell played a crucial role in facilitating fast oxygen dissociation. In this study, the effect of forming M@Pt (M core, Pt shell) particles for a range of metal cores (M = 3d, 4d, and 5d transition metals) is considered, with respect to O_2 dissociation on the Pt(111) facets. We show that forming M@Pt particles with late transition metal cores results in favorable shell flexibility for very low O_2 dissociation barriers. Conversely, alloying with early transition metals results in a more rigid Pt shell because of dominant M−Pt interactions, which prevent lowering of the dissociation barriers.

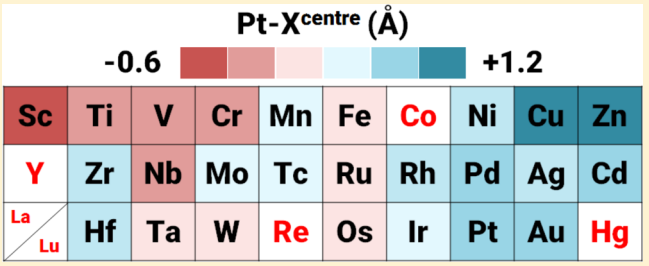

INTRODUCTION

The development of hydrogen fuel cells is a promising way to reduce the dependence of the energy sector on fossil fuels. Proton exchange membrane (PEM) fuel cells are ideally suited for transport and mobile auxiliary power applications as a result of their high power density, rapid start up and high efficiency.[1] These fuel cells are energy converting devices whereby electricity and heat are produced through an electrochemical process where the only waste product is water.

Pt-based catalysts are used in many industrial applications, catalyzing the oxygen reduction reaction (ORR) in PEM fuel cells being one of them.[2−4] Despite widespread utilization, for low temperature fuel cells, a common problem associated with the use of a Pt electrocatalyst is the strong Pt−O binding. This strong binding aids oxygen dissociation but is responsible for slowing down ORR kinetics.[5−7] Many studies have been reported modeling the overall mechanism of the ORR,[8−12] as well as chemisorption studies of specific intermediates within the reaction.[13−15] An example of this is the behavior of O_2 dissociation on Pt surfaces, which has been studied extensively. While this has predominantly focused on bulk systems,[16−23] some studies have been performed on small particles.[24−27]

The interest in interactions of oxygen species with platinum has resulted in numerous studies being performed on various extended Pt surfaces,[28−30] as well as studies of both free[31−33] and supported Pt particles[34,35] belonging to the size regime where "each atom counts".[36] Particle models expose a greater number and diversity of symmetry inequivalent sites to bind oxygen, when compared to slab models. For these particle structures, the under-coordinated surface atoms provide a variety of electronic environments at which to bind O.[37] While size effects are of interest, particularly at the subnanometer range,[38] it should be noted that it is also possible to use larger particle models that are scalable with size.[39−43]

A reduction of the dependence on Pt electrocatalysts in order to improve the commercial viability of PEM fuel cells has driven much research in the field. While a number of nonplatinum based systems have been proposed for potential use as PEM electrocatalysts,[44−46] there has been much focus on Pt-based binary[47,48] and ternary[49−51] alloys. Studies of platinum alloyed with both early[5,52] and late[53,54] transition metals have been performed. In this work, a range of possible binary systems with d-metal cores (groups 3−12 and 3d−5d metals of the periodic table) have been considered forming model M@Pt particles. Emphasis is placed on studying O_2 dissociation with special consideration of the effect the core metal plays on altering the dissociation barrier.

In previous work, we showed that when Pt is alloyed with titanium (Ti) to produce (Ti)core−(Pt)shell Ti@Pt moieties, changes in their electronic structure result in weaker Pt−O

Special Issue: Current Trends in Clusters and Nanoparticles Conference

Received: November 19, 2014
Revised: January 6, 2015
Published: January 7, 2015

DOI: 10.1021/jp511598e
J. Phys. Chem. C 2015, 119, 11031−11041

binding, through filling of the Pt *d*-band;[55,56] similar trends have been found for a number of other Pt-based alloy systems.[57−59] In later studies, it was found that while the strong core−shell interactions could result in a favorable reduction of Pt−O binding energies, these strong Pt−M interactions also partially disfavor oxygen dissociation. Shell flexibility plays an important role in facilitating fast oxygen dissociation: on pure Pt particles, the outermost shell can distort in such a way as to reduce the O_2 dissociation barrier from 0.4 eV on the (111) slab to <0.1 eV on the (111) facet of the particle.[60]

The previous studies on oxygen dissociation were performed on 38- and 79-atom particles. It is noted that other studies found a significant variation in adsorption energies of O on small Pt particles when nearby facets were modified by the presence of oxygen; although, this appears less pronounced for particles with about 80 or more atoms.[61] In our later work, O_2 dissociation studies were performed on the larger Pt_{116} nanoparticles, which should be in the range where properties scale with size.[39,62] These studies once again revealed the importance of shell flexibility in promoting fast O_2 dissociation on Pt particles.

There is much evidence that the formation of Pt alloys with late transition metals results in improved ORR kinetics;[63−65] although, this electrocatalytic improvement is often at the cost of long-term stability. It has been found that the compromised stability is the result of dealloying,[66,67] though there is much ongoing work to address this.[68−70] Pt alloys formed with early transition metals have been proposed to possess greater stability, although these particles are often more challenging to produce experimentally.[5,71]

The current study allows for the investigation of general trends across the groups of metals being investigated. This renders possible comparisons of both early and late transition metals, with the aim of discerning promising candidates for catalyzing the ORR in PEM fuel cells. While primarily focusing on the early stages of the ORR, namely, O_2 dissociation, the later stages are also considered by way of studying electronic changes induced by alloying through calculating shifts in the Pt *d*-band center.

METHODOLOGY

Calculations are performed using the Vienna Ab-Initio Simulation Package (VASP) 5.2.[72−75] All calculations are spin-polarized with valence electrons being treated explicitly, while the ionic cores are represented by the projected augmented wave (PAW) method.[76,77] Electronic exchange and correlation are described within the generalized gradient approximation (GGA) using the Perdew−Wang 91 (PW91) formula.[78,79] The Methfessel-Paxton smearing method is used with a width of 0.1 eV (extrapolated for computing final energies at zero smearing), and an energy cutoff of 415 eV for plane waves has been employed. All particles are placed in the center of large enough supercells to ensure sufficient separation between periodic images of roughly 10 Å. The Γ point is used to sample the Brillouin Zone. Atoms are relaxed according to the calculated forces, with convergence criteria for energies and forces required to be better than 1.0×10^{-4} eV/atom and 0.02 eV/Å, respectively.

Dissociation pathways are investigated using the VASP Transition State Tools (VTST) implementation of the VASP code by first generating an approximate pathway using the Nudged Elastic Band (NEB) method,[80] with further refinements achieved using the Dimer method.[81] Charges are calculated using the Bader method.[82,83]

In order to assess the (atomic or molecular) oxygen adsorption strength to the Pt surface, the binding (adsorption) energy (E_b) is calculated, as defined in eq 1.

$$E_b = E_{AB} - (E_A + E_B) \tag{1}$$

E_{AB} is the energy of the particle with an oxygen atom or molecule adsorbed, E_A is the energy of the relaxed bare particle, and E_B is the energy of the free oxygen atom or molecule. Negative E_b values characterize exothermic interactions. The interaction energy (E_{int}) is defined in eq 2.

$$E_{int} = E_{AB} - (E_A^* + E_B^*) \tag{2}$$

The single point energies of separate species A and B calculated at the geometries distorted upon adsorption are denoted by *; again, negative values imply favorable interactions. Distortion energies are defined according to eq 3.

$$\Delta E_A = E_A - E_A^* \tag{3}$$

Although specific distortions, brought about by adsorption of oxygen, are discussed in detail, as a more general measure, root mean squared displacements (RMSD) of atoms are calculated as defined in eq 4.

$$\mathrm{RMSD} = \sqrt{\frac{1}{N}\sum_{i}^{N}(\vec{m}_i - \vec{m}_i^*)^2} \tag{4}$$

N is the number of atoms under scrutiny in the metal particle, $\vec{m}_i$ is the position of a given atom in the relaxed bare particle, and $\vec{m}_i^*$ is the position of the same atom in the particle following oxygen adsorption. In all cases, RMSD values are calculated for atoms of the Pt shell, neglecting any displacement of core atoms. Prior to applying this equation, rotation and translation operators are applied to align each particle, thereby minimizing the RMSD. All RMSD values are positive, regardless of contraction or expansion of the particle, as they are averaged displacements in all directions and not associated with a displacement along a certain vector.

$Pt-X^{center}$ values are calculated to better understand the extent of (111) facet distortions. In the studies presented previously,[60,62] it was found that a reduction in the O_2 dissociation barrier was dependent on the extent to which the central atom of the (111) facet was "lifted" out of the plane. The vertical distance ("lifting") of the central atom relative to a plane is termed $Pt-X^{center}$. This ignores distortions in the plane and only accounts for distortions out of the plane, as shown in Figure 1.

The *d*-band center is a useful characteristic for relating changes in electronic properties of the particle to differences in, for example, O_2 binding energies. The *d*-band center (ϵ_d) is calculated, as in eq 5,

$$\epsilon_d = \frac{\int \rho E \mathrm{d}E}{\int \rho \mathrm{d}E} \tag{5}$$

where ρ is the *d*-band density of states, E is the *d*-band energy, and ρdE is the number of *d*-states.

RESULTS AND DISCUSSION

Geometric Analysis. The investigation of 38-atom M@Pt core−shell truncated octahedral (TO) particles is performed,

DOI: 10.1021/jp511598e
J. Phys. Chem. C 2015, 119, 11031−11041

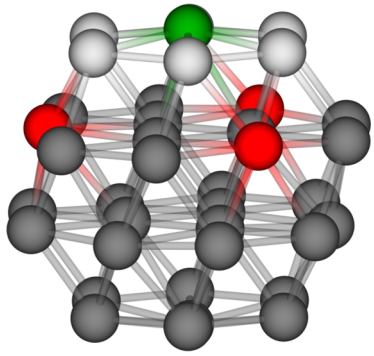

Figure 1. To measure distortion of a particular facet (e.g., of light gray atoms), Pt−X^{center} values are calculated. This is achieved by defining a plane that passes through the center of the adjoining (111) facets (red atoms), then measuring the distance by which the central (111) atom (green atom) is lifted out of the plane.

with analysis of the data presented in Table 1. It should be noted that the 38-atom particle size corresponds to a magic number for the TO structure, constituting a complete 6-atom core and a 32-atom shell. From our previous studies, it is apparent that weaker core−shell interactions facilitate the surface flexibility that is beneficial for fast O_2 dissociation. When considering a wider range of M@Pt d-metal core−shell particles, it is likely to be beneficial for M atoms of the core to have a similar electronegativity to Pt. Pt has an electronegativity of 2.28 on the Pauling scale (Table 1) compared to 1.54 for Ti in Ti@Pt particles investigated previously.[60] With Pt and Ti having such different electronegativities, it is to be expected that there will be quite strong core−shell interactions with a large charge transfer, which is indeed the case.[60]

Figure 2a shows that in general, moving from early to late d-metals is coupled with an increase in electronegativity, while moving from 3d to 5d metals results in less well-defined trends. This suggests that late d-metals are likely to result in the desirable weaker core−shell interactions. Studies have shown that alloys formed between platinum and early transition metals are particularly stable, a result of the strong Pt−M interactions.[5] To test this, binding energies were calculated for Pt−M dimers. From Figure 2b it is also possible to see a strong correlation between the metal group and the Pt−M binding energy. It is evident that late d-metals have significantly reduced binding energies compared to early metals. Furthermore, there appears to be little period dependence.

Most of the d-metals investigated in this study could form particles with a TO structure;[87−91] however, it is noted that, for a large mismatch in the Pt/M atomic radii, the TO structure may be destabilized. In this study, the TO structure is used as a model in order to compare the reactivity of different metal cores toward O_2 dissociation, even though the TO is not always the lowest energy structure. When performing geometry optimizations on the bare 38-atom particles, all M@Pt compositions minimize to the TO structure, apart from the Co@Pt system, which is found to distort away from the TO toward the octahedral−icosahedral (Oh-Ih) structure.[92] Indeed, previous studies have revealed that the TO structure is not favorable for the Co@Pt particle.[93]

The RMSD for the Pt shell was calculated by comparing the Pt shell of the pure Pt_{38} particle with the Pt shell of the M@Pt core−shell particle, the results of which are shown in Table 1 and plotted in Figure 2c. The RMSD values give an indication of how changing the metal core affects the Pt shell, large values indicate significant distortion of the Pt shell, while small values indicate that changing the core has little effect on the Pt shell. Large RMSD values are generally calculated for the particles with early d-metal cores, while there is a general reduction of the RMSD for late d-metals. Furthermore, moving from 3d to 5d leads to a reduction in the RMSD. This shows that the Pt shells of particles formed with late d-metal cores, particularly for those located close to Pt in the periodic table, are more structurally similar to that of the Pt_{38} particle. Structural similarities between the Pt_{38} and M@Pt particles could potentially be an important consideration, indicating a preference toward favorable distortion of the (111) terrace upon adsorption of O_2.

The RMSD will not only be influenced by $E_b[M]$, but also by the atomic radius of the alloyed element. It is likely that deviation from the approximate atomic radii of Pt (1.36 Å) will result in strain because of the size mismatch between the core and the shell. The atomic radii of the various elements are shown in Table 1, where it is seen that progression from early to late transition metals leads to the well-known general decrease in atomic radii. Concomitantly, moving from 3d to 5d metals, results in a general expansion of the atomic radii. Strain also has an effect on the binding energy of adsorbates, where an increase in the Pt−Pt bond length will result in stronger

Table 1. Electronegativity (χ)[84,85] of the Metals M in M@Pt Core, Pt−M Dimer Binding Energy ($E_b[M]$) in eV, Calculated Atomic Radii of M[86] in Å, and RMSD Values in Å of the Pt Shell Associated with All Systems Investigated

3d metals					4d metals					5d metals				
M@Pt	χ	$E_b[M]$	atomic radii	RMSD	M@Pt	χ	$E_b[M]$	atomic radii	RMSD	M@Pt	χ	$E_b[M]$	atomic radii	RMSD
										La	1.10	−3.94	2.07	0.24
Sc	1.36	−4.22	1.70	0.09	Y	1.22	−4.28	1.90	0.18	Lu	1.27	−3.34	1.87	0.14
Ti	1.54	−4.18	1.60	0.15	Zr	1.33	−4.40	1.75	0.14	Hf	1.30	−5.61	1.75	0.14
V	1.63	−4.30	1.53	0.24	Nb	1.60	−4.34	1.64	0.19	Ta	1.50	−4.82	1.70	0.19
Cr	1.66	−4.49	1.39	0.13	Mo	2.16	−4.31	1.54	0.15	W	2.36	−4.73	1.62	0.21
Mn	1.55	−4.67	1.39	0.14	Tc	1.90	−4.18	1.47	0.13	Re	1.90	−4.53	1.51	0.12
Fe	1.83	−3.85	1.32	0.15	Ru	2.20	−3.45	1.46	0.10	Os	2.20	−3.75	1.44	0.11
Co	1.88	−2.98	1.26	-[a]	Rh	2.28	−2.87	1.42	0.06	Ir	2.20	−3.00	1.41	0.05
Ni	1.91	−2.36	1.24	0.14	Pd	2.20	−2.24	1.39	0.06	Pt	2.28	−2.38	1.36	0.00
Cu	1.90	−1.77	1.32	0.16	Ag	1.93	−1.49	1.45	0.07	Au	2.54	−1.49	1.36	0.06
Zn	1.65	−1.13	1.22	0.14	Cd	1.69	−0.98	1.44	0.08	Hg	2.00	−1.45	1.32	0.09

[a]TO structure lost completely during local relaxation.

DOI: 10.1021/jp511598e
J. Phys. Chem. C 2015, 119, 11031−11041

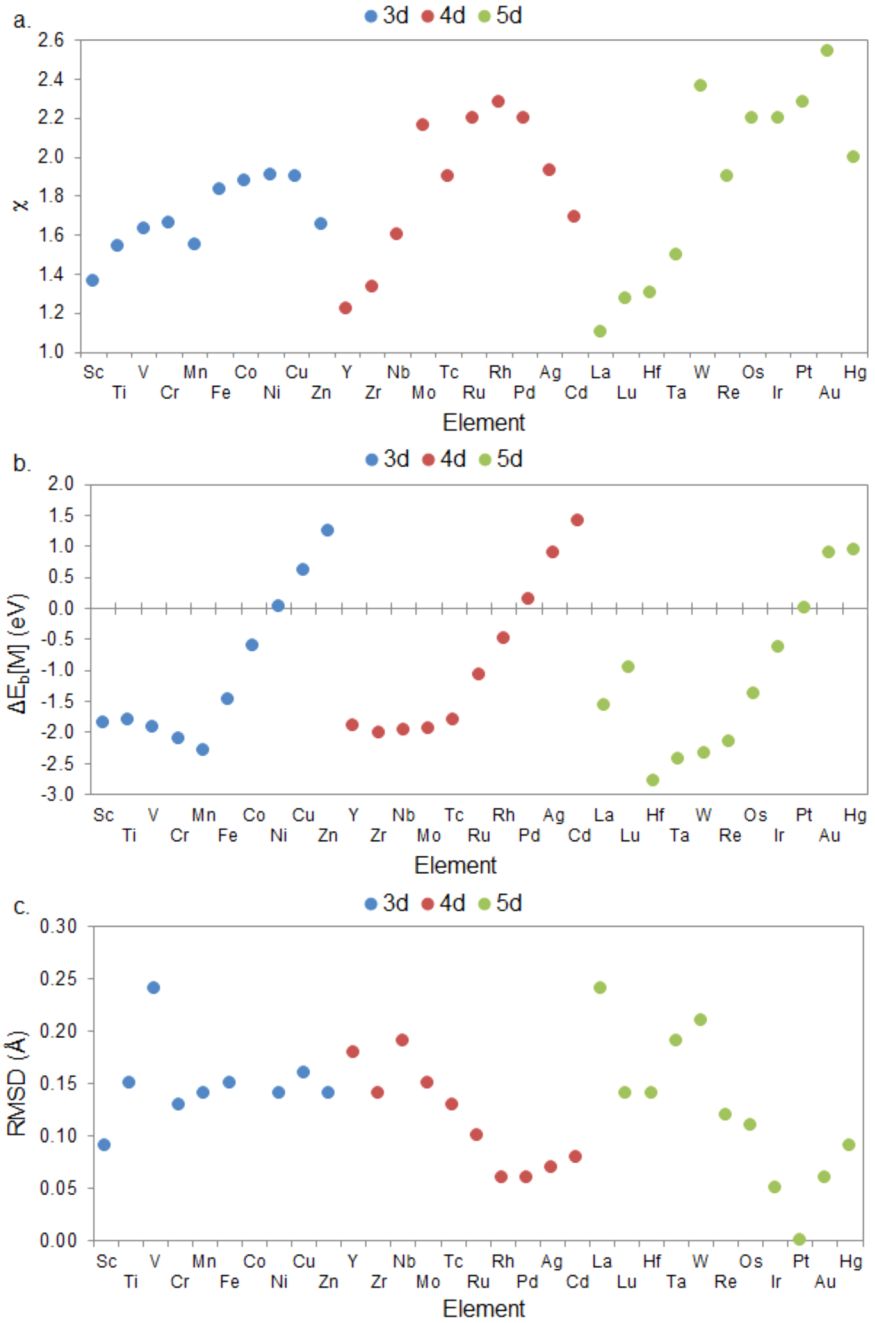

Figure 2. (a) Plot of electronegativity values χ across the range of studied d-metals.[84,85] (b) Pt−M dimer binding energies $\Delta E_b[M]$, relative to Pt_2, calculated for the range of studied d-metals. (c) RMSD values calculated for the Pt shell of the 38-atom M@Pt particles for the range of studied d-metals.

binding, and a decrease will lead to a weakening of adsorbate binding.[94−97] Discussions on the relationship between the electronegativity and the Pt−M binding energy and Pt−M binding energy and the RMSD are given in the Supporting Information, Figure S1.

O_2 Chemisorption Studies. Sites 6 (3-fold *hcp* hollow) and 7 (3-fold *fcc* hollow) on the 38-atom M@Pt TO particles are investigated (Figure 3). Geometric representations of the particles are provided in the Supporting Information, Figures S2−S7. More detailed discussions of distortions induced upon adsorption of O_2 are presented in the following. When O_2 is adsorbed at site 6, for 3d metals, it is found that there is noticeable distortion of the (111) facet for the Sc@Pt particle, while there is little distortion of the (111) facet for metals M of groups 4−8. Co was not investigated because during the relaxation of the bare particle, the structure dramatically distorted from the TO. For M of groups 10−12, similar distortions of the (111) facet to those of the pure Pt particle are observed. For the same groups, when O_2 is adsorbed on site 7, there is spontaneous dissociation of the O_2 molecule. The O_2 dissociation barrier on the Pt_{38} particle for site 7 is very slightly smaller than that for site 6.[60] It could therefore be expected that the dissociation barriers at sites 7 on the M@Pt particles are also slightly lower than those for site 6. It follows that, where the Pt−M binding energies are reduced compared to those for

DOI: 10.1021/jp511598e
J. Phys. Chem. C 2015, 119, 11031−11041

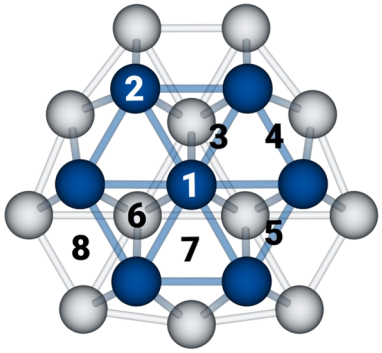

Figure 3. Top view of the surface (dark blue) and subsurface (light gray) metal atoms at a (111) facet showing symmetry inequivalent adsorption sites for the 38-atom TO particle.

Pt−Pt, the activation barrier at site 7 indicates spontaneous dissociation.

Considering distortion of the M@Pt particles, it is apparent that upon adsorption of O_2, 4d M@Pt particles exhibit similar behavior to those of 3d metals, although now group 9 can be investigated, with Rh@Pt locally minimizing to the TO structure. One interesting difference between 3d and 4d metals is that, while the Y@Pt particle distorts from the TO structure, with the core atoms occupying surface sites to form a Y−O bond, the Zr@Pt alloy exhibits (111) facet distortions very similar to those of the Pt_{38} particle. The distortion of the Y@Pt particle is likely the result of two effects. First, Y has an atomic radii of 1.90 Å, compared to 1.36 Å for Pt, suggesting that the Pt surface will experience tensile strain. Indeed, a relatively large RMSD of 0.18 Å is calculated for Y@Pt (Table 1). Second, early transition metals, such as Y, form very strong M−O bonds. It is likely that the increased atomic radius of Y coupled with tensile strain on the Pt shell means that the core atoms are more accessible for oxygen (both O and O_2) to interact with, allowing for stronger M−O interactions than with the Pt shell.

The behavior of the Zr@Pt particle is in stark contrast to the Ti@Pt particle. From Table 1 it can be seen that there is a strong Pt−Zr dimer binding of −4.40 eV, which is in fact stronger than that of the Pt−Ti binding of −4.18 eV. The other early d-metal particles exhibit similar properties to those in group 4, where there is little distortion of the (111) facet upon adsorption of O_2. The (111) facets of the Rh@Pt particles are found to distort rather strongly, as is the case with groups 10−12. Once again, spontaneous O_2 dissociation is noticeable on site 7 for group 9−12 metals, as well as Zr. Some distortions are observed for earlier metals, although these seem to be related to instabilities in the TO structures, with some tending toward, for example, icosahedral structures. However, these distortions are not the favorable (111) facet distortions that are of interest in this study.

Similar trends to those observed for 3d and 4d metals are also inherent for 5d metals. Distortions of the central atom of the (111) facet are notable for the later d-metals (groups 9−12), while there is little distortion for earlier d-metals. The La@Pt particle distorts upon O_2 binding in a similar fashion to Y@Pt, where the core atoms are pulled to surface sites forming a La−O bond. For 5d metals, it is also found that the Hg@Pt particle distorts away from the TO when O_2 is adsorbed on site 6. Spontaneous O_2 dissociation occurs on site 7 for Ir@Pt, Au@Pt, and Hg@Pt, although this was not the case for Pt_{38}.[60]

From the study of O_2 adsorption on the 38-atom M@Pt particles, several trends become apparent. The late d-metals from groups 9−12 appear to be the most promising candidates for fast O_2 dissociation. In all cases where weaker Pt−M binding is found, compared to that of Pt−Pt, distortions of the (111) facet are observed, though, it is also found that the Rh and Ir systems, with stronger Pt−M binding by ≤0.62 eV compared to Pt−Pt binding, as well as exhibit surface distortion by O_2. However, particles with Pt−M binding energies ≥1.07 eV do not exhibit this behavior. Thus, the structural flexibility of the particle changes with Pt−M binding energies somewhere between 0.6 and 1.1 eV greater than that for Pt−Pt binding. All structures can be found in the Supporting Information, Figures S2−S7.

The binding energies for O_2 adsorption on sites 6 and 7 are presented in Table 2. In general, later d-metal systems, for which Pt shell distortions are observed, bind O_2 stronger than earlier d-metal systems, where distortions to the (111) facet are not noticeable. This is likely because of two effects: First, the distorted (111) facet will provide a more favorable surface for O_2 to bind. Second, *d*-band characteristics will affect O_2 binding energy. As the Pt *d*-band is filled, the corresponding downshift in the *d*-center will result in weakening of the O_2 binding.[98] Pt alloyed with later d-metals does not yield a downshift in the *d*-center and will more likely result in an upshift. This upshift in the Pt *d*-center will probably also contribute to the increased O_2 binding energies for later M@Pt particles.

Charge density difference plots for O_2 adsorption on sites 6 and 7 are included in the Supporting Information, Figures S8−

Table 2. O_2 Binding Energy Values in eV (E_b) for Adsorption on Sites 6 and 7 on the Range of M@Pt Particles

3d-M@Pt	site 6	site 7	4d-M@Pt	site 6	site 7	5d-M@Pt	site 6	site 7
						La	[a]	[a]
Sc	−1.22	−0.79	Y	[a]	[a]	Lu	[a]	[a]
Ti	−0.77	−0.40	Zr	−1.11	−2.46	Hf	−0.95	−0.43
V	−0.89	−0.77	Nb	−0.79	−0.67	Ta	−0.77	−0.66
Cr	−0.96	−0.64	Mo	−2.01	−2.14	W	−1.91	−0.91
Mn	−2.06	−1.69	Tc	−1.69	−3.03	Re	−3.75	−3.09
Fe	−0.91	−0.48	Ru	−1.34	−1.40	Os	−1.54	−1.10
Co	[b]	[b]	Rh	−1.26	−2.21	Ir	−1.24	−2.22
Ni	−1.99	−4.00	Pd	−1.26	−2.34	Pt	−1.80	−1.76
Cu	−1.18	−2.56	Ag	−1.18	−2.20	Au	−1.36	−2.34
Zn	−1.52	−2.55	Cd	−1.55	−2.26	Hg	−5.16	−2.48

[a]Structure strongly distorted such that oxygen is bound to the core atoms. [b]TO structure completely lost during local relaxation prior to O_2 adsorption.

DOI: 10.1021/jp511598e
J. Phys. Chem. C 2015, 119, 11031−11041

S13. These are generated by subtracting the charge (electron) densities of M@Pt and O_2 (or O + O) fragments from that of the total M@Pt−O_2 system. The charge densities of the M@Pt and O_2 fragments are calculated with the positions of atoms optimized for the total system. The plots show little difference for particles with cores of early and late transition metals.

Distortion Studies. The calculated values for RMSD and Pt−X^{center}, characterizing particle distortion upon O_2 adsorption are listed in Table 3. The RMSD vales in Table 3 are calculated for the Pt shell, following adsorption of O_2, differing from those listed in Table 1, calculated for the Pt shell of the particle prior to adsorption of O_2. Several systems exhibit very large RMSD values of ∼0.5 Å and above, these large values are the result of structural rearrangements away from the TO shape, for example, Y, La, Re, and Hg. For those structures that do not break the model TO shape upon adsorption of O_2, the later d-metals tend to have larger RMSD values compared to particles containing early d-metals. The difference in RMSD values between particles containing early and late d-metal cores is the result of distortions of the (111) facet, particularly around the central atom. There also tend to be larger RMSD values associated with site 7 compared to those for site 6. This is because of the large distortions resulted from the spontaneous O_2 dissociation found at site 7.

Table 3. RMSD of the Pt Shell Following O_2 Adsorption and Pt−X^{center} for the Bare Particle as Well as Relative Pt−X^{center} Following O_2 Adsorption on Sites 6 and 7 for the Range of M@Pt Particles[a]

	RMSD		Pt−X^{center}		
3d-M@Pt	site 6	site 7	bare	site 6	site 7
Sc	0.18	0.25	2.38	−0.62	−0.38
Ti	0.03	0.06	2.27	−0.08	−0.15
V	0.05	0.07	2.13	−0.04	−0.06
Cr	0.05	0.08	2.27	−0.10	−0.15
Mn	0.06	0.09	2.24	0.06	0.01
Fe	0.03	0.07	2.24	−0.01	−0.04
Co	[b]	[b]	[b]	[b]	[b]
Ni	0.54	0.68	2.27	0.10	
Cu	0.21	0.50	2.24	1.14	1.28
Zn	0.30	0.43	2.25	1.21	1.34
	RMSD		Pt−X^{center}		
4d-M@Pt	site 6	site 7	bare	site 6	site 7
Y	0.61	0.49	2.48	[c]	[c]
Zr	0.17	0.43	2.38	0.36	[c]
Nb	0.04	0.08	2.27	−0.10	−0.08
Mo	0.14	0.26	2.25	0.01	−0.10
Tc	0.06	0.55	2.27	0.07	[c]
Ru	0.04	0.24	2.31	−0.01	0.03
Rh	0.05	0.28	2.36	0.20	1.12
Pd	0.24	0.31	2.37	0.98	1.13
Ag	0.08	0.29	2.37	0.32	1.08
Cd	0.22	0.31	2.40	0.89	1.09
	RMSD		Pt−X^{center}		
5d-M@Pt	site 6	site 7	bare	site 6	site 7
La	0.54	0.62	2.56	[c]	[c]
Lu	0.57	0.35	2.42	[c]	[c]
Hf	0.16	0.19	2.68	0.33	−0.18
Ta	0.04	0.08	2.25	−0.09	−0.09
W	0.25	0.07	2.19	−0.07	−0.05
Re	0.45	0.55	2.29	[c]	[c]
Os	0.04	0.06	2.30	−0.01	−0.03
Ir	0.04	0.29	2.38	0.05	1.11
Pt	0.20	0.20	2.44	0.82	0.83
Au	0.19	0.28	2.41	0.79	1.02
Hg	0.98	0.31	2.46	[c]	1.01

[a]All values are in Å; a negative Pt−X^{center} value corresponds to particle contraction, whereas a positive value shows particle expansion. [b]TO structure lost during local relaxation prior to O_2 adsorption. [c]Structure strongly distorted such that no meaningful value could be calculated.

In Table 3, negative Pt−X^{center} values show that there has been a displacement of the central (111) atom toward the particle core. Conversely, a positive Pt−X^{center} value shows that the central atom has moved away from the particle core. Distortions of the (111) facet resulting in a positive Pt−X^{center} value are of interest for faster O_2 dissociation.[60] Generally, when O_2 is adsorbed on M@Pt particles with early d-metals, there is a contraction in Pt−X^{center}. For the M@Pt particles with late d-metals, there is generally an expansion of Pt−X^{center}, comparable to Pt_{38}. Clusters with strong core−shell Pt−M binding show a contraction of the Pt shell upon adsorption of O_2, whereas an expansion of the Pt shell takes place for M@Pt systems with weaker core−shell interactions; this trend is shown in Figure 4.

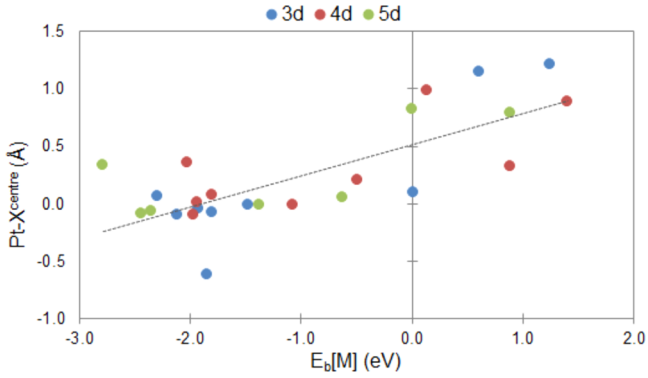

Figure 4. Plot of the Pt−M binding energy ($E_b[M]$) and Pt−X^{center} on the range of M@Pt particles, the R^2 of the data is 0.58.

Figure 5 shows the relationship between Pt−X^{center} and the binding energy of O_2 to the studied M@Pt particles. For site 6, there is no clear trend, suggesting that distortions of the (111) facet do not lead to significantly stronger O_2 adsorption. For site 7 there is a more obvious trend. In this case, the M@Pt particles that result in spontaneous O_2 dissociation exhibit significantly stronger O_2−M@Pt binding. However, the values of Pt−X^{center} for those particles where distortions of the (111) facet are observed, do not vary significantly for O_2 adsorbed at site 6 or 7. While there is generally little difference in binding energies between sites 6 and 7 for the early d-metals, there are significant differences for the later d-metals, where stronger binding is found at site 7. For completeness, the relationship between RMSD and the O_2 adsorption energies is shown in the Supporting Information, Figure S14.

Density of States Analysis. Calculated *d*-band center values of Pt in M@Pt particles may give an indication of ORR kinetics. It is expected that a downshift in Pt *d*-center (away from the Fermi energy) will result in weakening of molecular (e.g., OH, O_2) interactions with the Pt shell. Conversely, an upshift in the *d*-center (toward the Fermi energy) will likely

DOI: 10.1021/jp511598e
J. Phys. Chem. C 2015, 119, 11031−11041

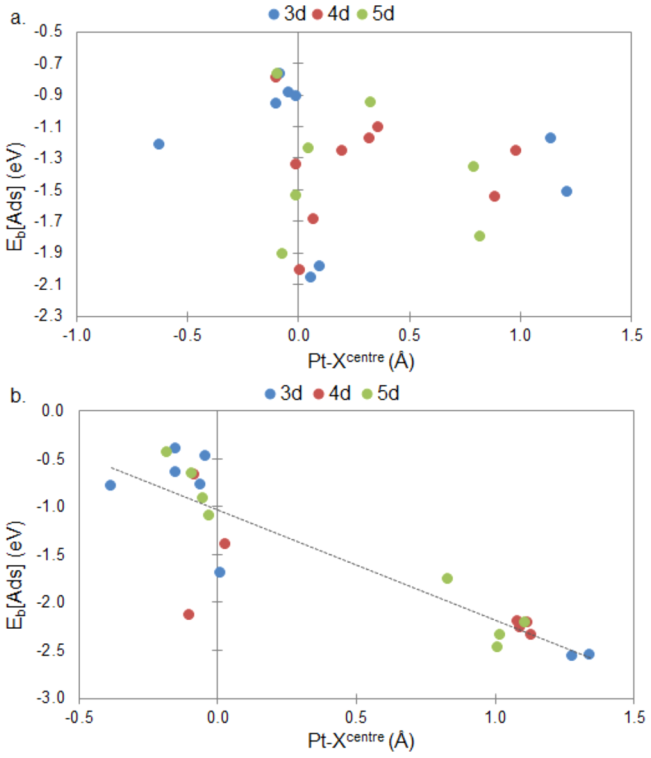

Figure 5. Plot of Pt−X^{center} and O_2 binding energies for sites 6 (a) and 7 (b) on the range of M@Pt particles. There is no general trend for the data presented on binding to site 6, while the R^2 of the data for binding on site 7 is 0.78.

result in strengthening of these interactions.[98] It is known that stronger Pt−O interactions lead to lower dissociation barriers of O_2,[99] which is in conflict with the need for reduced Pt−O binding to allow for desorption of oxygen containing species and formation, for example of H_2O from OH + H.

In Figure 6, the *d*-center position of the Pt shell for varying compositions is plotted relative to that of the outer shell in the pure Pt_{38} particle. In general, when Pt is alloyed with early d-metals, significant downshifts in the *d*-center are observed. For the later d-metals (around group 10) the shifts in the *d*-center become less negative (or in some cases positive with an upshift). The *d*-band center shifts are the result of electronic and geometric effects.[100] For the early d-metals, it is likely that electronic effects dominate the changes in Pt *d*-band characteristics, where significant charge transfer is observed between the M core and the Pt shell. For the later d-metals, where there is less charge transfer, it is likely that geometric effects have an increased importance in determining changes in the Pt *d*-center.

It is expected that group 9 metals (Co, Rh, Ir) in M@Pt could be a promising compromise between the ability to dissociate O_2 and later desorb the resulting products. These metals exhibit a slight downshift in the Pt *d*-band center, by 0.1 eV, in line with results found elsewhere.[101] Furthermore, alloying Pt with group 9 metals simultaneously allows for favorable distortions of the (111) facet. These metals form slightly stronger Pt−M bonds than Pt−Pt. It most likely facilitates the greater shift in Pt *d*-band center but the bonding is not strong enough to inhibit distortion of the (111) facet.

Potential M@Pt Candidates for Replacement of Pure Pt in Catalysts for O_2 Dissociation and Oxygen Reduction. Investigation of O_2 dissociation has been performed on a number of promising M@Pt candidates, showing favorable (111) distortions during the chemisorption studies. As discussed in previous sections, Pt-based alloys formed with late transition metals provide the most promising candidates. Thus, our focus was placed on M@Pt particles with metals of groups 9−12. Although, alloys formed from group 9 metals were of particular interest for the O_2 dissociation studies, the Co@Pt system is not investigated as already explained, because the TO structure is not its local minimum. Small O_2 dissociation barriers relating to other promising M@Pt combinations are as follows (in eV): 0.06 for Cu, 0.07 for Rh, 0.04 for Pd, 0.01 for Cd, and 0.27 for Ir. This compares with a barrier of 0.04 eV for the pure Pt_{38} TO particle.[60] Graphical representations of the initial, transition, and final states (IS, TS, and FS, respectively) are collected in the Supporting Information, Figures S15−S20.

Pt−Cu alloys have been demonstrated to exhibit favorable ORR reaction kinetics.[102,103] In the initial stages of O_2 chemisorption, there was significant distortion of the (111) facet. The O_2 dissociation barrier on site 6 is 0.06 eV, while spontaneous O_2 dissociation was found at site 7 assisted by geometry relaxation. This is in line with the O_2 dissociation barrier at position 6 on Pt_{38}, which is 0.04 eV.[60] It is therefore corroborated that the Cu@Pt particle displays favorable properties for O_2 dissociation as the pure Pt system does. However, from the investigations of Pt *d*-band center, there is very little difference between the pure Pt and Cu@Pt particles. This implies that the Cu@Pt particle is also likely to overbind oxygen species, inhibiting the later stages of the ORR. Copper is significantly cheaper than platinum, at a cost of around £5.00

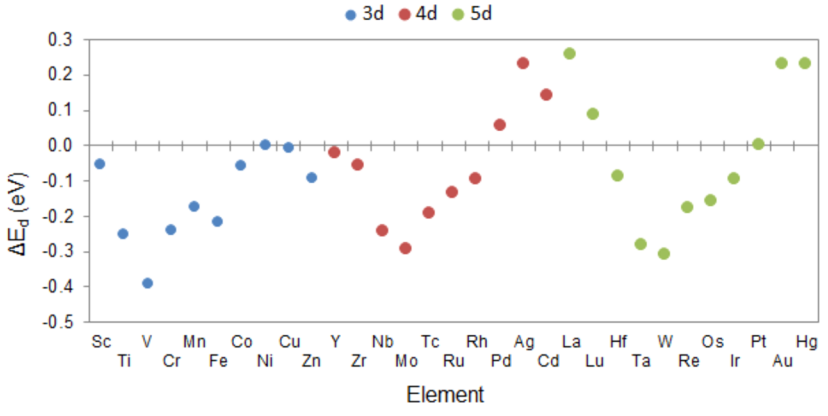

Figure 6. Variation of calculated Pt *d*-band centers ΔE_d for the range of M@Pt particles, relative to that of Pt_{38} particle.

DOI: 10.1021/jp511598e
J. Phys. Chem. C 2015, 119, 11031−11041

kg^{-1} and £28.00 g^{-1} (all prices quoted here and in the following are as of June 2014), respectively.[104] This means that formidable cost reductions could be made through usage of Cu@Pt electrocatalysts.

Pt−Rh alloys have been considered for fuel cell applications,[105] although Rh costs £21.00 g^{-1},[104] so there would be relatively little cost reduction through alloying. As stated previously, the TO Rh@Pt moiety demonstrates favorable (111) facet distortions when O_2 is adsorbed. When a transition state search is performed on site 6, a dissociation barrier of 0.07 eV is found. Again, this is in line with the O_2 dissociation barrier at position 6 on the Pt_{38} particle. When investigating site 7, as the Rh@Pt−O_2 system is locally relaxed, the O_2 molecule dissociates. This suggests that the distortion of the (111) facets spontaneously overcomes the small O_2 dissociation barrier which has been observed previously. Furthermore, there is a slight downshift in the Pt *d*-center of the Rh@Pt particle, meaning that the latter has a potential not only to exhibit fast O_2 dissociation kinetics but also improve overall ORR kinetics when compared to the pure Pt system.

A similar trend is found for Pt alloyed with Pd and Cd, where the O_2 dissociation barriers at site 6 are 0.04 and 0.01 eV, respectively. At site 7, spontaneous dissociation is calculated for both systems. For Pd@Pt, there is a slight upshift in Pt *d*-band center, of 0.06 eV, while for the Cd@Pt particle, there is a greater upshift in the Pt *d*-band center by 0.14 eV. This suggests that, while O_2 dissociation may be fast, it is probable that later ORR kinetics would be slowed down. The cost of Pd is £14.00 g^{-1},[104] though Cd costs significantly less, at £2.00 kg^{-1}.[106] However, it should be noted that Cd is extremely toxic, meaning that the suitability of Cd@Pt nanoparticles for commercial applications would be highly questionable.

The Pt−Ir system is slightly different from the others, with an O_2 dissociation barrier of 0.27 eV for site 6 and spontaneous dissociation calculated at site 7. A barrier of 0.27 eV is still below that for the bulk Pt system (∼0.40 eV), although it is not as low as for other systems that have been investigated. However, the Ir@Pt system does have a downshift in the Pt *d*-band center by 0.1 eV, which could suggest that the alloyed system has advantages over the pure Pt system. Furthermore, the price of Ir is £9.00 g^{-1},[104] which could still provide a reduction in the cost of the electrocatalyst.

CONCLUSIONS

It has been shown that favorable distortions of the (111) facet of small metal particles, to facilitate O_2 dissociation are not confined to the pure Pt particles. Late d-metals with relatively weak Pt−M interactions also exhibit this behavior. Furthermore, the weakened core−shell interactions in the M@Pt particles facilitate O_2 dissociation to give very low dissociation barriers of <0.1 eV. Note, however, that we did not explicitly address stability of the bimetallic Pt−M particles in the presence of O_2 atmosphere, which may be another crucial limitation of applications of these systems as ORR catalysts. Of the systems studied, each has distinct advantages and disadvantages for ORR associated with it, meaning the most promising system will have to be a compromise between the different characteristics being investigated. The best candidates should have large flexibility of the surface (111) facets, which ensures fast O_2 dissociation and downshift of the *d*-band center, allowing easier desorption of oxygen containing species in the next steps of the ORR process.

Group 9 metals appear to provide the most promising compromise, whereby there is a slight downshift in the Pt *d*-band center for the M@Pt particles compared to the pure Pt particles. Furthermore, there are favorable distortions of the (111) facet induced by the binding of O_2, which subsequently results in very low O_2 dissociation barriers. This suggests that, while the initial stages of the ORR (O_2 dissociation) will not be hindered by a rigid (111) facet, the kinetics of the later stages will be improved compared to the pure Pt particle. Furthermore, the Pt−M binding energy is slightly greater than the Pt−Pt binding energy, suggesting that these bimetallic particles with group 9 metals may have improved stability over the alloys formed with other late transition metals.

It is worth noting that an O_2 dissociation barrier of ∼0.4 eV, such as that for Pt (111) slab, is already relatively low and should allow for high reactivity. The current work has not only focused on reducing this small barrier further, but also on improving selectivity toward the dissociative four electron pathway of the ORR.

ASSOCIATED CONTENT

Supporting Information

Further details from the Geometric Analysis and Distortion Studies sections, as well as graphical geometric representations of systems being investigated and charge density difference plots. This material is available free of charge via the Internet at http://pubs.acs.org.

AUTHOR INFORMATION

Corresponding Authors

*E-mail: konstantin.neyman@icrea.cat.

*E-mail: r.l.johnston@bham.ac.uk.

Present Address

‡Department of Energy Conversion and Storage, Technical University of Denmark, Roskilde, Denmark (P.C.J.).

Notes

The authors declare no competing financial interest.

ACKNOWLEDGMENTS

This research was funded through the RCUK doctoral training centre in hydrogen, fuel cells, and their applications (EP/G037116/1). Financial support was also provided by the EU (FP7-NMP.2012.1.1-1 Project ChipCAT, ref. No. 310191), the Generalitat de Catalunya (2014SGR97, XRQTC), and the Spanish MICINN (CTQ2012-34969). The authors thank COST Actions CM1104 and MP0903. Much of the initial work was performed under the HPC-EUROPA2 Project (Project No.: 228398) with the support of the European Commission - Capacities Area - Research Infrastructures. The computations described in this paper were performed in part using The University of Birmingham's BlueBEAR HPC service, which was purchased through HEFCE SRIF-3 funds and via our membership of the U.K.'s HPC Materials Chemistry Consortium, which is funded by EPSRC (EP/F067496). This work made use of the facilities of HECToR, the U.K.'s national high-performance computing service, which is provided by UoE HPCx Ltd. at the University of Edinburgh, Cray Inc., and NAG Ltd., and funded by the Office of Science and Technology through EPSRC's High End Computing Programme. H.A.A. thanks the Spanish Ministerio de Educación for a postdoctoral grant (SB2010-0172), Bulgarian Science Fund (Grant DCVP 02/1), and FP7 project BeyondEverest for support.

DOI: 10.1021/jp511598e
J. Phys. Chem. C 2015, 119, 11031−11041

REFERENCES

(1) Chandan, A.; Hattenberger, M.; El-kharouf, A.; Du, S.; Dhir, A.; Self, V.; Pollet, B. G.; Ingram, A.; Bujalski, W. High Temperature (HT) Polymer Electrolyte Membrane Fuel Cells (PEMFC) - A Review. *J. Power Sources* **2013**, *231*, 264−278.

(2) Guo, S.; Zhang, S.; Sun, S. Tuning Nanoparticle Catalysis for the Oxygen Reduction Reaction. *Angew. Chem., Int. Ed.* **2013**, *52*, 8526−8544.

(3) Liu, Z.; Ma, L.; Zhang, J.; Hongsirikarn, K.; Goodwin, J. G. Pt Alloy Electrocatalysts for Proton Exchange Membrane Fuel Cells: A Review. *Catal. Rev.* **2013**, *55*, 255−288.

(4) Su, L.; Jia, W.; Li, C.-M.; Lei, Y. Mechanisms for Enhanced Performance of Platinum-Based Electrocatalysts in Proton Exchange Membrane Fuel Cells. *ChemSusChem* **2014**, *7*, 361−378.

(5) Greeley, J.; Stephens, I. E. L.; Bondarenko, A. S.; Johansson, T. P.; Hansen, H. A.; Jaramillo, T. F.; Rossmeisl, J.; Chorkendorff, I.; Nørskov, J. K. Alloys of Platinum and Early Transition Metals as Oxygen Reduction Electrocatalysts. *Nat. Chem.* **2009**, *1*, 552−556.

(6) Viswanathan, V.; Hansen, H. A.; Rossmeisl, J.; Nørskov, J. K. Universality in Oxygen Reduction Electrocatalysis on Metal Surfaces. *ACS Catal.* **2012**, *2*, 1654−1660.

(7) Johansson, T. P.; Ulrikkeholm, E. T.; Hernandez-Fernandez, P.; Malacrida, P.; Hansen, H. A.; Bandarenka, A. S.; Nørskov, J. K.; Rossmeisl, J.; Stephens, I. E. L.; Chorkendorff, I. Pt Skin Versus Pt Skeleton Structures of Pt3Sc as Electrocatalysts for Oxygen Reduction. *Top. Catal.* **2013**, *57*, 245−254.

(8) Anderson, A. B.; Albu, T. V. Catalytic Effect of Platinum on Oxygen Reduction an Ab Initio Model Including Electrode Potential Dependence. *J. Electrochem. Soc.* **2000**, *147*, 4229−4238.

(9) Jinnouchi, R. New Insight Into Microscale Transport Phenomena In PEFC By Quantum MD. *Microscale Thermophys. Eng.* **2003**, *7*, 15−31.

(10) Nørskov, J. K.; Rossmeisl, J.; Logadottir, A.; Lindqvist, L.; Kitchin, J. R.; Bligaard, T.; Jónsson, H. Origin of the Overpotential for Oxygen Reduction at a Fuel-Cell Cathode. *J. Phys. Chem. B* **2004**, *108*, 17886−17892.

(11) Keith, J. A.; Jerkiewicz, G.; Jacob, T. Theoretical Investigations of the Oxygen Reduction Reaction on Pt(111). *ChemPhysChem* **2010**, *11*, 2779−2794.

(12) Sha, Y.; Yu, T. H.; Merinov, B. V.; Shirvanian, P.; Goddard, W. A. Oxygen Hydration Mechanism for the Oxygen Reduction Reaction at Pt and Pd Fuel Cell Catalysts. *J. Phys. Chem. Lett.* **2011**, *2*, 572−576.

(13) Koper, M. T. M.; Shubina, T. E.; van Santen, R. A. Periodic Density Functional Study of CO and OH Adsorption on Pt-Ru Alloy Surfaces: Implications for CO Tolerant Fuel Cell Catalysts. *J. Phys. Chem. B* **2002**, *106*, 686−692.

(14) Seminario, J.; Agapito, L.; Yan, L.; Balbuena, P. Density Functional Theory Study of Adsorption of OOH on Pt-Based Bimetallic Clusters Alloyed with Cr, Co, and Ni. *Chem. Phys. Lett.* **2005**, *410*, 275−281.

(15) Han, B.; Miranda, C.; Ceder, G. Effect of Particle Size and Surface Structure on Adsorption of O and OH on Platinum Nanoparticles: A First-Principles Study. *Phys. Rev. B* **2008**, *77*, 075410.

(16) Getman, R. B.; Xu, Y.; Schneider, W. F. Thermodynamics of Environment-Dependent Oxygen Chemisorption on Pt(111). *J. Phys. Chem. C* **2008**, *112*, 9559−9572.

(17) Smeltz, A.; Getman, R.; Schneider, W.; Ribeiro, F. Coupled Theoretical and Experimental Analysis of Surface Coverage Effects in Pt-Catalyzed NO and O_2 Reaction to NO_2 on Pt(111). *Catal. Today* **2008**, *136*, 84−92.

(18) Getman, R.; Schneider, W.; Smeltz, A.; Delgass, W.; Ribeiro, F. Oxygen-Coverage Effects on Molecular Dissociations at a Pt Metal Surface. *Phys. Rev. Lett.* **2009**, *102*, 076101.

(19) Chen, W.; Schmidt, D.; Schneider, W. F.; Wolverton, C. Ordering and Oxygen Adsorption in Au−Pt/Pt(111) Surface Alloys. *J. Phys. Chem. C* **2011**, *115*, 17915−17924.

(20) Bray, J. M.; Schneider, W. F. Potential Energy Surfaces for Oxygen Adsorption, Dissociation, and Diffusion at the Pt(321) Surface. *Langmuir* **2011**, *27*, 8177−8186.

(21) Fu, Q.; Yang, J.; Luo, Y. A First Principles Study on the Dissociation and Rotation Processes of a Single O_2 Molecule on the Pt(111) Surface. *J. Phys. Chem. C* **2011**, *115*, 6864−6869.

(22) Stamatakis, M.; Vlachos, D. G. Unraveling the Complexity of Catalytic Reactions via Kinetic Monte Carlo Simulation: Current Status and Frontiers. *ACS Catal.* **2012**, *2*, 2648−2663.

(23) Schmidt, D. J.; Chen, W.; Wolverton, C.; Schneider, W. F. Performance of Cluster Expansions of Coverage-Dependent Adsorption of Atomic Oxygen on Pt(111). *J. Chem. Theory Comput.* **2012**, *8*, 264−273.

(24) Xu, Y.; Shelton, W. A.; Schneider, W. F. Effect of Particle Size on the Oxidizability of Platinum Clusters. *J. Phys. Chem. A* **2006**, *110*, 5839−5846.

(25) Lim, D.-H.; Wilcox, J. DFT-Based Study on Oxygen Adsorption on Defective Graphene-Supported Pt Nanoparticles. *J. Phys. Chem. C* **2011**, *115*, 22742−22747.

(26) Kettner, M.; Schneider, W. B.; Auer, A. A. Computational Study of Pt/Co Core−Shell Nanoparticles: Segregation, Adsorbates and Catalyst Activity. *J. Phys. Chem. C* **2012**, *116*, 15432−15438.

(27) Cheng, D.; Wang, W. Tailoring of Pd−Pt Bimetallic Clusters with High Stability for Oxygen Reduction Reaction. *Nanoscale* **2012**, *4*, 2408−2415.

(28) Ge, Q.; Hu, P.; King, D. A.; Lee, M.-H.; White, J. A.; Payne, M. C. Site Symmetry Dependence of Repulsive Interactions Between Chemisorbed Oxygen Atoms on Pt{100}-(11). *J. Chem. Phys.* **1997**, *106*, 1210.

(29) Bleakley, K.; Hu, P. A Density Functional Theory Study of the Interaction between CO and O on a Pt Surface: CO/Pt(111), O/Pt(111), and CO/O/Pt(111). *J. Am. Chem. Soc.* **1999**, *121*, 7644−7652.

(30) Tang, H.; Van der Ven, A.; Trout, B. Phase Diagram of Oxygen Adsorbed on Platinum (111) by First-Principles Investigation. *Phys. Rev. B* **2004**, *70*, 045420.

(31) Lin, X.; Ramer, N. J.; Rappe, A. M.; Hass, K. C.; Schneider, W. F.; Trout, B. L. Effect of Particle Size on the Adsorption of O and S Atoms on Pt: A Density-Functional Theory Study. *J. Phys. Chem. B* **2001**, *105*, 7739−7747.

(32) Li, T.; Balbuena, P. B. Computational Studies of the Interactions of Oxygen with Platinum Clusters. *J. Phys. Chem. B* **2001**, *105*, 9943−9952.

(33) Jacob, T.; Muller, R. P.; Goddard, W. A. Chemisorption of Atomic Oxygen on Pt(111) from DFT Studies of Pt-Clusters. *J. Phys. Chem. B* **2003**, *107*, 9465−9476.

(34) Vayssilov, G. N.; Lykhach, Y.; Migani, A.; Staudt, T.; Petrova, G. P.; Tsud, N.; Skála, T.; Bruix, A.; Illas, F.; Prince, K. C.; et al. Support Nanostructure Boosts Oxygen Transfer to Catalytically Active Platinum Nanoparticles. *Nat. Mater.* **2011**, *10*, 310−315.

(35) Nguyen, T. Q.; Escaño, M. C. S.; Nakanishi, H.; Kasai, H.; Maekawa, H.; Osumi, K.; Sato, K. DFT+U Study on the Oxygen Adsorption and Dissociation on CeO_2-Supported Platinum Cluster. *Appl. Surf. Sci.* **2014**, *288*, 244−250.

(36) Heiz, U.; Sanchez, A.; Abbet, S.; Schneider, W.-D. Catalytic Oxidation of Carbon Monoxide on Monodispersed Platinum Clusters: Each Atom Counts. *J. Am. Chem. Soc.* **1999**, *121*, 3214−3217.

(37) Johnston, R. L. *Atomic and Molecular Clusters*; Taylor & Francis: London, 2002; p 208.

(38) Vajda, S.; Pellin, M. J.; Greeley, J. P.; Marshall, C. L.; Curtiss, L. A.; Ballentine, G. A.; Elam, J. W.; Catillon-Mucherie, S.; Redfern, P. C.; Mehmood, F.; et al. Subnanometre Platinum Clusters as Highly Active and Selective Catalysts for the Oxidative Dehydrogenation of Propane. *Nat. Mater.* **2009**, *8*, 213−216.

(39) Kozlov, S. M.; Neyman, K. M. Catalysis from First Principles: Towards Accounting for the Effects of Nanostructuring. *Top. Catal.* **2013**, *56*, 867−873.

(40) Aleksandrov, H. A.; Viñes, F.; Ludwig, W.; Schauermann, S.; Neyman, K. M. Tuning the Surface Chemistry of Pd by Atomic C and H: A Microscopic Picture. *Chem.—Eur. J.* **2013**, *19*, 1335−1345.

(41) Viñes, F.; Lykhach, Y.; Staudt, T.; Lorenz, M. P. A.; Papp, C.; Steinrück, H.-P.; Libuda, J.; Neyman, K. M.; Görling, A. Methane

DOI: 10.1021/jp511598e
J. Phys. Chem. C 2015, 119, 11031−11041

Activation by Platinum: Critical Role of Edge and Corner Sites of Metal Nanoparticles. *Chem.—Eur. J.* **2010**, *16*, 6530−6539.
(42) Kozlov, S. M.; Aleksandrov, H. A.; Neyman, K. M. Adsorbed and Subsurface Absorbed Hydrogen Atoms on Bare and MgO(100)-Supported Pd and Pt Nanoparticles. *J. Phys. Chem. C* **2014**, *118*, 15242−15250.
(43) Aleksandrov, H. A.; Kozlov, S. M.; Schauermann, S.; Vayssilov, G. N.; Neyman, K. M. How Absorbed Hydrogen Affects the Catalytic Activity of Transition Metals. *Angew. Chem., Int. Ed.* **2014**, *53*, 13371−13375.
(44) Olson, T. S.; Chapman, K.; Atanassov, P. Non-Platinum Cathode Catalyst Layer Composition for Single Membrane Electrode Assembly Proton Exchange Membrane Fuel Cell. *J. Power Sources* **2008**, *183*, 557−563.
(45) Feng, Y.; Gago, A.; Timperman, L.; Alonso-Vante, N. Chalcogenide Metal Centers for Oxygen Reduction Reaction: Activity and Tolerance. *Electrochim. Acta* **2011**, *56*, 1009−1022.
(46) Wu, G.; More, K. L.; Johnston, C. M.; Zelenay, P. High-Performance Electrocatalysts for Oxygen Reduction Derived from Polyaniline, Iron, and Cobalt. *Science* **2011**, *332*, 443−447.
(47) Marković, N. M.; Schmidt, T. J.; Stamenković, V.; Ross, P. N. Oxygen Reduction Reaction on Pt and Pt Bimetallic Surfaces: A Selective Review. *Fuel Cells* **2001**, *1*, 105−116.
(48) Strasser, P. Dealloyed Core-Shell Fuel Cell Electrocatalysts. *Rev. Chem. Eng.* **2009**, *25*, 255−295.
(49) Zhong, C.-J.; Luo, J.; Njoki, P. N.; Mott, D.; Wanjala, B.; Loukrakpam, R.; Lim, S.; Wang, L.; Fang, B.; Xu, Z. Fuel Cell Technology: Nano-Engineered Multimetallic Catalysts. *Energy Environ. Sci.* **2008**, *1*, 454.
(50) Wang, C.; van der Vliet, D.; More, K. L.; Zaluzec, N. J.; Peng, S.; Sun, S.; Daimon, H.; Wang, G.; Greeley, J.; Pearson, J.; et al. Multimetallic Au/$FePt_3$ Nanoparticles as Highly Durable Electrocatalyst. *Nano Lett.* **2011**, *11*, 919−926.
(51) Wang, C.; Li, D.; Chi, M.; Pearson, J.; Rankin, R. B.; Greeley, J.; Duan, Z.; Wang, G.; van der Vliet, D.; More, K. L.; et al. Rational Development of Ternary Alloy Electrocatalysts. *J. Phys. Chem. Lett.* **2012**, *3*, 1668−1673.
(52) Stephens, I. E. L.; Bondarenko, A. S.; Bech, L.; Chorkendorff, I. Oxygen Electroreduction Activity and X-Ray Photoelectron Spectroscopy of Platinum and Early Transition Metal Alloys. *ChemCatChem* **2012**, *4*, 341−349.
(53) di Paola, C.; Baletto, F. Oxygen Adsorption on Small PtNi Nanoalloys. *Phys. Chem. Chem. Phys.* **2011**, *13*, 7701−7707.
(54) Zhang, L.; Iyyamperumal, R.; Yancey, D. F.; Crooks, R. M.; Henkelman, G. Design of Pt-Shell Nanoparticles with Alloy Cores for the Oxygen Reduction Reaction. *ACS Nano* **2013**, *7*, 9168−9172.
(55) Jennings, P. C.; Pollet, B. G.; Johnston, R. L. Theoretical Studies of Pt-Ti Nanoparticles for Potential use as PEMFC Electrocatalysts. *Phys. Chem. Chem. Phys.* **2012**, *14*, 3134−3139.
(56) Jennings, P. C.; Pollet, B. G.; Johnston, R. L. Electronic Properties of Pt−Ti Nanoalloys and the Effect on Reactivity for Use in PEMFCs. *J. Phys. Chem. C* **2012**, *116*, 15241−15250.
(57) Hammer, B.; Nørskov, J. Electronic Factors Determining the Reactivity of Metal Surfaces. *Surf. Sci.* **1995**, *343*, 211−220.
(58) Stamenkovic, V. R.; Mun, B. S.; Arenz, M.; Mayrhofer, K. J. J.; Lucas, C. A.; Wang, G.; Ross, P. N.; Markovic, N. M. Trends in Electrocatalysis on Extended and Nanoscale Pt-Bimetallic Alloy Surfaces. *Nat. Mater.* **2007**, *6*, 241−247.
(59) Yoo, S. J.; Hwang, S. J.; Lee, J.-G.; Lee, S.-C.; Lim, T.-H.; Sung, Y.-E.; Wieckowski, A.; Kim, S.-K. Promoting Effects of La for Improved Oxygen Reduction Activity and High Stability of Pt on Pt-La Alloy Electrodes. *Energy Environ. Sci.* **2012**, *5*, 7521−7525.
(60) Jennings, P. C.; Aleksandrov, H. A.; Neyman, K. M.; Johnston, R. L. A DFT Study of Oxygen Dissociation on Platinum Based Nanoparticles. *Nanoscale* **2014**, *6*, 1153−1165.
(61) Larsen, A. H.; Kleis, J.; Thygesen, K. S.; Nørskov, J. K.; Jacobsen, K. W. Electronic Shell Structure and Chemisorption on Gold Nanoparticles. *Phys. Rev. B* **2011**, *84*, 245429.
(62) Jennings, P. C.; Aleksandrov, H.; Neyman, K. M.; Johnston, R. L. DFT Studies of Oxygen Dissociation on the 116-Atom Platinum Truncated Octahedron Particle. *Phys. Chem. Chem. Phys.* **2014**, *16*, 26539−26545.
(63) Debe, M. K. Electrocatalyst Approaches and Challenges for Automotive Fuel Cells. *Nature* **2012**, *486*, 43−51.
(64) Gasteiger, H. A.; Kocha, S. S.; Sompalli, B.; Wagner, F. T. Activity Benchmarks and Requirements for Pt, Pt-Alloy, and Non-Pt Oxygen Reduction Catalysts for PEMFCs. *Appl. Catal. B: Environ.* **2005**, *56*, 9−35.
(65) Stephens, I. E. L.; Bondarenko, A. S.; Grønbjerg, U.; Rossmeisl, J.; Chorkendorff, I. Understanding the Electrocatalysis of Oxygen Reduction on Platinum and its Alloys. *Energy Environ. Sci.* **2012**, *5*, 6744.
(66) Maillard, F.; Dubau, L.; Durst, J.; Chatenet, M.; André, J.; Rossinot, E. Durability of Pt_3Co/C Nanoparticles in a Proton-Exchange Membrane Fuel Cell: Direct Evidence of Bulk Co Segregation to the Surface. *Electrochem. Commun.* **2010**, *12*, 1161−1164.
(67) Chen, S.; Gasteiger, H. A.; Hayakawa, K.; Tada, T.; Shao-Horn, Y. Platinum-Alloy Cathode Catalyst Degradation in Proton Exchange Membrane Fuel Cells: Nanometer-Scale Compositional and Morphological Changes. *J. Electrochem. Soc.* **2010**, *157*, A82.
(68) Sasaki, K.; Naohara, H.; Choi, Y.; Cai, Y.; Chen, W.-F.; Liu, P.; Adzic, R. R. Highly Stable Pt Monolayer on PdAu Nanoparticle Electrocatalysts for the Oxygen Reduction Reaction. *Nat. Commun.* **2012**, *3*, 1115−1124.
(69) Wang, D.; Xin, H. L.; Hovden, R.; Wang, H.; Yu, Y.; Muller, D. A.; DiSalvo, F. J.; Abruña, H. D. Structurally Ordered Intermetallic Platinum-Cobalt Core-Shell Nanoparticles with Enhanced Activity and Stability as Oxygen Reduction Electrocatalysts. *Nat. Mater.* **2013**, *12*, 81−87.
(70) Cui, C.; Gan, L.; Heggen, M.; Rudi, S.; Strasser, P. Compositional Segregation in Shaped Pt Alloy Nanoparticles and their Structural Behaviour during Electrocatalysis. *Nat. Mater.* **2013**, *12*, 765−771.
(71) Hernandez-Fernandez, P.; Masini, F.; McCarthy, D. N.; Strebel, C. E.; Friebel, D.; Deiana, D.; Malacrida, P.; Nierhoff, A.; Bodin, A.; Wise, A. M.; et al. Mass-Selected Nanoparticles of Pt_xY as Model Catalysts for Oxygen Electroreduction. *Nat. Chem.* **2014**, DOI: 10.1038/nchem.2001.
(72) Kresse, G.; Hafner, J. Ab Initio Molecular Dynamics for Liquid Metals. *Phys. Rev. B* **1993**, *47*, 558−561.
(73) Kresse, G. Efficient Iterative Schemes for Ab Initio Total-Energy Calculations Using a Plane-Wave Basis Set. *Phys. Rev. B* **1996**, *54*, 11169−11186.
(74) Kresse, G.; Furthmüller, J. Efficiency of Ab-Initio Total Energy Calculations for Metals and Semiconductors using a Plane-Wave Basis Set. *Comput. Mater. Sci.* **1996**, *6*, 15−50.
(75) Kresse, G.; Hafner, J. Ab initio Molecular-Dynamics Simulation of the Liquid-Metal Amorphous-Semiconductor Transition in Germanium. *Phys. Rev. B* **1994**, *49*, 14251−14269.
(76) Kresse, G. From Ultrasoft Pseudopotentials to the Projector Augmented-Wave Method. *Phys. Rev. B* **1999**, *59*, 1758−1775.
(77) Blöchl, P. E. Projector Augmented-Wave Method. *Phys. Rev. B* **1994**, *50*, 17953−17979.
(78) Perdew, J. P.; Jackson, K. A.; Pederson, M. R.; Singh, D. J.; Fiolhais, C.; Chevary, J.; Vosko, S. Erratum: Atoms, molecules, solids, and surfaces: Applications of the generalized gradient approximation for exchange and correlation. *Phys. Rev. B* **1992**, *46*, 6671−6687.
(79) Perdew, J.; Chevary, J.; Vosko, S.; Jackson, K.; Pederson, M.; Singh, D.; Fiolhais, C. Erratum: Atoms, Molecules, Solids, and Surfaces: Applications of the Generalized Gradient Approximation for Exchange and Correlation. *Phys. Rev. B* **1993**, *48*, 4978−4978.
(80) Sheppard, D.; Xiao, P.; Chemelewski, W.; Johnson, D. D.; Henkelman, G. A Generalized Solid-State Nudged Elastic Band Method. *J. Chem. Phys.* **2012**, *136*, 074103.
(81) Kästner, J.; Sherwood, P. Superlinearly Converging Dimer Method for Transition State Search. *J. Chem. Phys.* **2008**, *128*, 014106.

DOI: 10.1021/jp511598e
J. Phys. Chem. C 2015, 119, 11031−11041

(82) Bader, R. F. W. *Atoms in Molecules: a Quantum Theory*; Oxford University Press: New York, 1994.
(83) Tang, W.; Sanville, E.; Henkelman, G. A Grid-Based Bader Analysis Algorithm without Lattice Bias. *J. Phys.: Condens. Matter* **2009**, *21*, 084204.
(84) Pauling, L. *The Nature of the Chemical Bond and the Structure of Molecules and Crystals: An Introduction to Modern Structural Chemistry*; Cornell University Press: New York, 1960; p 644.
(85) Allred, A. Electronegativity Values from Thermochemical Data. *J. Inorg. Nucl. Chem.* **1961**, *17*, 215−221.
(86) Cordero, B.; Gómez, V.; Platero-Prats, A. E.; Revés, M.; Echeverra, J.; Cremades, E.; Barragán, F.; Alvarez, S. Covalent Radii Revisited. *Dalton Trans.* **2008**, 2832−8.
(87) Wu, J.; Yang, H. Synthesis and Electrocatalytic Oxygen Reduction Properties of Truncated Octahedral Pt3Ni Nanoparticles. *Nano Res.* **2010**, *4*, 72−82.
(88) Wu, J.; Zhang, J.; Peng, Z.; Yang, S.; Wagner, F. T.; Yang, H. Truncated Octahedral Pt(3)Ni Oxygen Reduction Reaction Electrocatalysts. *J. Am. Chem. Soc.* **2010**, *132*, 4984−4985.
(89) Narayanan, R.; El-Sayed, M. A. Shape-Dependent Catalytic Activity of Platinum Nanoparticles in Colloidal Solution. *Nano Lett.* **2004**, *4*, 1343−1348.
(90) Massen, C.; Mortimer-Jones, T. V.; Johnston, R. L. Geometries and Segregation Properties of Platinum-Palladium Nanoalloy Clusters. *J. Chem. Soc., Dalton Trans.* **2002**, 4375.
(91) Chu, Y.-Y.; Wang, Z.-B.; Dai, Z.; Gu, D.-M.; Yin, G.-P. Synthesis of Truncated-Octahedral Pt-Pd Nanocrystals Supported on Carbon Black as a Highly Efficient Catalyst for Methanol Oxidation. *Fuel Cells* **2014**, *14*, 49−55.
(92) Paz-Borbón, L. O.; Johnston, R. L.; Barcaro, G.; Fortunelli, A. Structural Motifs, Mixing, and Segregation Effects in 38-Atom Binary Clusters. *J. Chem. Phys.* **2008**, *128*, 134517.
(93) Barcaro, G.; Ferrando, R.; Fortunelli, A.; Rossi, G. Exotic Supported CoPt Nanostructures: From Clusters to Wires. *J. Phys. Chem. Lett.* **2010**, *1*, 111−115.
(94) Greeley, J.; Nørskov, J. K. A General Scheme for the Estimation of Oxygen Binding Energies on Binary Transition Metal Surface Alloys. *Surf. Sci.* **2005**, *592*, 104−111.
(95) Strasser, P.; Koh, S.; Anniyev, T.; Greeley, J.; More, K.; Yu, C.; Liu, Z.; Kaya, S.; Nordlund, D.; Ogasawara, H.; et al. Lattice-Strain Control of the Activity in Dealloyed Core-Shell Fuel Cell Catalysts. *Nat. Chem.* **2010**, *2*, 454−460.
(96) Mavrikakis, M.; Hammer, B.; Nørskov, J. Effect of Strain on the Reactivity of Metal Surfaces. *Phys. Rev. Lett.* **1998**, *81*, 2819−2822.
(97) Kitchin, J.; Nørskov, J.; Barteau, M.; Chen, J. Role of Strain and Ligand Effects in the Modification of the Electronic and Chemical Properties of Bimetallic Surfaces. *Phys. Rev. Lett.* **2004**, *93*, 156801.
(98) Chorkendorff, I.; Niemantsverdriet, J. W. *Concepts of Modern Catalysis and Kinetics*, 2nd ed.; Wiley-VCH Verlag GmbH & Co. KGaA: New York, 2006.
(99) Šljivančanin, Ž.; Hammer, B. Oxygen Dissociation at Close-Packed Pt Terraces, Pt Steps, and Ag-Covered Pt Steps Studied with Density Functional Theory. *Surf. Sci.* **2002**, *515*, 235−244.
(100) Kitchin, J.; Nørskov, J.; Barteau, M.; Chen, J. Role of Strain and Ligand Effects in the Modification of the Electronic and Chemical Properties of Bimetallic Surfaces. *Phys. Rev. Lett.* **2004**, *93*, 156801.
(101) Zhang, J.; Vukmirovic, M. B.; Xu, Y.; Mavrikakis, M.; Adzic, R. R. Controlling the Catalytic Activity of Platinum-Monolayer Electrocatalysts for Oxygen Reduction with Different Substrates. *Angew. Chem., Int. Ed.* **2005**, *44*, 2132−2135.
(102) Mani, P.; Srivastava, R.; Strasser, P. Dealloyed Binary PtM3 (M = Cu, Co, Ni) and Ternary PtNi3M (M = Cu, Co, Fe, Cr) Electrocatalysts for the Oxygen Reduction Reaction: Performance in Polymer Electrolyte Membrane Fuel Cells. *J. Power Sources* **2011**, *196*, 666−673.
(103) Mani, P.; Srivastava, R.; Strasser, P. Dealloyed Pt-Cu Core-Shell Nanoparticle Electrocatalysts for Use in PEM Fuel Cell Cathodes. *J. Phys. Chem. C* **2008**, *112*, 2770−2778.
(104) http://www.infomine.com/investment/metal-prices/ (accessed June 2014).
(105) Choi, J.-H.; Park, K.-W.; Park, I.-S.; Nam, W.-H.; Sung, Y.-E. Methanol Electro-Oxidation and Direct Methanol Fuel Cell Using Pt/Rh and Pt/Ru/Rh Alloy Catalysts. *Electrochim. Acta* **2004**, *50*, 787−790.
(106) http://www.metalprices.com/p/CadmiumFreeChart (accessed June 2014).

DOI: 10.1021/jp511598e
J. Phys. Chem. C 2015, 119, 11031−11041